ANNUAL JOURNAL OF ELECTRONICS, 2009, ISSN 1313-1842

Investigation and Analysis of Gyroscope MEMS Design Solutions for Automotive Applications

Malinka Spasova Ivanova, Manuela Marinova Nakova, Ivan Nikolaev Ivanov and Krassimir Hristov Denishev

Abstract – **In the paper the investigation on the gyroscope rate microelectromechanical systems (MEMS) with the application in the automotive industry is presented. The design solutions of 2-DOF (degree of freedom), 3-DOF and 4-DOF devices are explored and summarized. The method for design of vibratory rate gyroscope MEMS is proposed and the design steps are explored and analyzed.**

Keywords – **Gyroscope, MEMS, 4-DOF, automotive applications, design steps, bulk micromachining**

I. INTRODUCTION

The gyroscope microelectromechanical systems (GMEMS) with their reduced cost, size, and weight and increased performance find more and more adoption in the 3D input devices, robotics, platform stability, virtual reality, in the medicine, and everyday electronics [1], [2]. The investigation shows that the gyroscope MEMS are also suitable for automotive industry applications, such as: navigation and guidance systems, ride stabilization, advanced automotive safety systems like yaw and tilt control, roll-over detection and prevention, and next generation airbag and anti-lock brake systems [3]. The contemporary micromachining processes and the fabrication techniques allow the detection and control electronics to be integrated on the same silicon chip, together with the mechanical sensor elements. Thus, miniaturization of vibratory gyroscopes with innovative micro-fabrication processes and gyroscope designs is expected to become an attractive solution to current and future automotive market needs. Also, the professionals are looking for methods for their performance increase.

According to the performance of gyroscope MEMS, they can be classified into three different categories: inertial grade, tactical grade, and rate grade (gyroscope MEMS).

TABLE 1. PERFORMANCE REQUIREMENT FOR GYROSCOPE MEMS

Parameter	*Rate grade*	*Tactical Grade*	*Inertial Grade*
Angle Random Walk, °/√h	>0.5	0.5-0.05	<0.001
Bias Drift, °/h	10-1000	0.1-10	<0.01
Scale Factor Accuracy, %	0.1-1	0.01-0.1	<0.001
Full Scale Range (°/sec)	50-1000	>500	>400
Bandwidth, Hz	>70	100	100

K. Denishev, M. Nakova, I. Ivanov are with the Department of Microelectronics, Faculty of Electronic Engineering and Technologies, Technical University - Sofia, 8 Kliment Ohridski blvd., 1000 Sofia, Bulgaria, e-mail: khd@tu-sofia.bg

M. Ivanova is with the College of Energetics and Electronics, Technical University - Sofia, 8 Kliment Ohridski blvd., 1000 Sofia, Bulgaria, e-mail: m_ivanova@tu-sofia.bg

The parameters' comparison among these devices is shown in Table 1. Over the past decade, much of the effort in developing silicon GMEMS has concentrated on rate grade devices, which are useful for automotive applications. These automotive devices generally require robust yet sensitive gyroscopes with operational frequencies above several kHz in order to suppress the effect of environmental vibrational noise, the desired mechanical bandwidth of the sense mode is typically between 100 Hz - 400Hz, the operating temperature is in the range from -40 to 85° C. One challenging problem is how wide bandwidth frequency responses in the drive and sense modes of the vibratory gyroscopes to be achieved.

In the paper, the dynamic systems' design concepts with different degree of freedom (DOF) of the drive and sense mode were investigated and analyzed in point of view the GMEMS performance improvement. The method for design of vibratory rate gyroscope MEMS is examined and the design steps are explored and summarized.

II. DESIGN CONCEPTS OF VIBRATORY RATE GYROSCOPE MEMS

2-DOF rate gyroscope MEMS operates on the vibratory principle with a single proof mass, suspended above the substrate. The 3-DOF gyroscope MEMS design concept is based on utilizing resonance in the one of the modes by forming structurally decoupled 2-DOF and 1-DOF oscillators in the drive and sense modes. The 4-DOF gyroscope MEMS design approach is based on forming a 2-DOF drive-mode oscillator and a 2-DOF sense-mode oscillator, using three interconnected proof masses [4], [5], [6]. In the following sections, the design concepts of 2-DOF, 3-DOF and 4-DOF dynamical systems are examined.

A. Dynamical System with 2-DOF Design Concept

At the 2-DOF rate gyroscope MEMS, the proof mass is free to oscillate in two orthogonal directions: the drive - direction x and the sense - direction y (Figure 1).

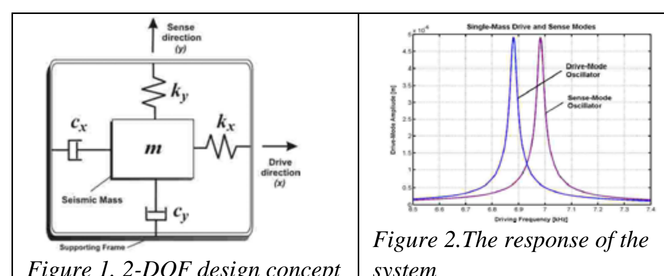

Figure 1. 2-DOF design concept

Figure 2. The response of the system

An external sinusoidal force, generally, the electrostatic one is applied by comb-drive structures and put the proof mass into resonance in the drive direction. When the gyroscope performs angular rotation, the Coriolis force is induced in the y direction. If the drive and sense resonant frequencies are matched, the Coriolis force excites the system into resonance in the sense direction. The resulting oscillation amplitude in the sense direction is proportional to the Coriolis force and, thus, to the angular velocity to be measured. The sense direction oscillation is detected generally by air-gap capacitors. To achieve the maximum possible gain, the conventional gyroscopes are generally designed to operate at or near the peak of the response curve (Figure 2). This is typically achieved by matching drive and sense resonant frequencies.

B. Dynamical System with 3-DOF Design Concept

The 3-DOF design concept aims to utilize resonance in either the drive mode or the sense mode, to improve sensitivity while maintaining the robust operational characteristics. For this purpose, structurally decoupled 2-DOF and 1-DOF oscillators are formed in the drive and sense modes (Figure 3). The 2-DOF oscillator frequency response is characterized with two resonance peaks, and a flat region between the peaks, that defines the operation frequency region (Figure 4). The 1-DOF oscillator resonant frequency is designed to overlap with the drive mode flat operating region. In this way, the device is operated at the resonant frequency of the 1-DOF oscillator for improved sensitivity, while 2-DOF oscillator amplitude is inherently constant within the same frequency band.

In the 3-DOF system with 2-DOF drive mode, the wide-band region is achieved in the drive-mode frequency response. By utilizing dynamic amplification in the drive-mode, large oscillation amplitudes of the sensing element is achieved with small actuation amplitudes, providing improved linearity and stability even with parallel plate actuation.

In the 3-DOF system with 2-DOF sense mode, the wide-band region is obtained in the sense mode frequency response, and the device is operated at resonance in the drive mode. This allows utilization of well-proven drive-mode control techniques, while providing robust gain and phase in the sense mode.

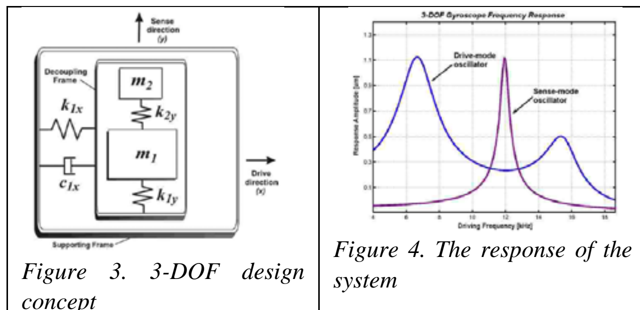

Figure 3. 3-DOF design concept

Figure 4. The response of the system

C. Dynamical System with 4-DOF Design Concept

The 4-DOF dynamical system is designed with three interconnected proof masses, which provides the flexibility in defining the drive and sense mode dynamical parameters independently (Figure 5). The approach is based on utilizing a 2-DOF drive-direction oscillator and a 2-DOF sense-direction oscillator, that form a 4-DOF overall dynamical system; in contrast to the conventional gyroscope approach with a 2-DOF overall dynamical system. The frequency responses of the drive and sense direction oscillators have two resonant peaks and a flat region between the peaks (Figure 6). The device is operated in the flat regions of the response curves belonging to the drive and sense direction oscillators, where the gain is less sensitive to frequency fluctuations.

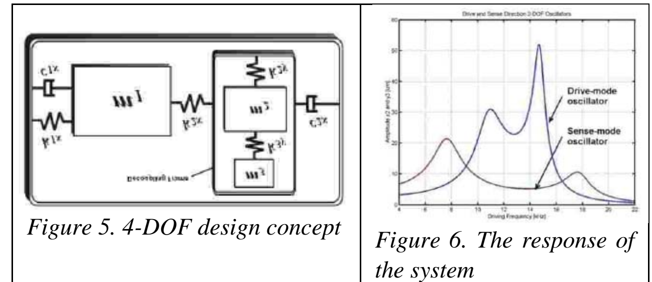

Figure 5. 4-DOF design concept

Figure 6. The response of the system

III. Design Method of Vibratory Rate Gyroscope MEMS

The explored literature sources show a wide range of mechanical structures, actuation and detection schemes, and fabrication technologies for the GMEMS. Despite of this, the major design issues of microelectromechanical vibratory systems are presented in Figure 7.

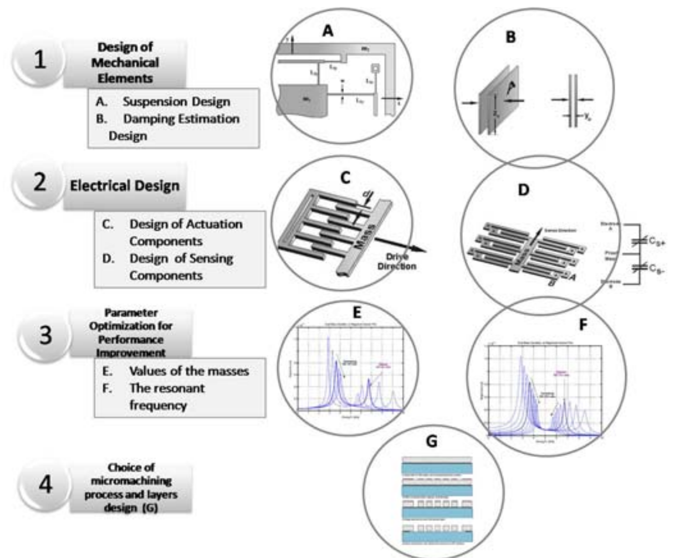

Figure 7. Design Method

IV. Design of 4-DOF Gyroscope MEMS

The 4-DOF solution proposes dynamical amplification in the 2-DOF oscillators instead of resonance, increased bandwidth and reduced sensitivity to structural and thermal parameter fluctuations [7], [8].

The 4-DOF system consists of 3-mass approaches. The mass m_1 with 1-DOF is free to oscillate only in the drive direction. The mass m_2 has 2-DOF, oscillating in both drive

and sense directions, and the mass m_3 with 1-DOF is fixed with respect to m_2 in the drive direction, and free to oscillate independently in the sense direction (Figure 8).

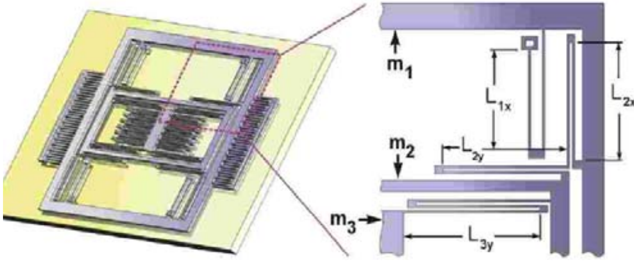

Figure 8. 4-DOF System

A.Design of Mechanical Elements

Suspension Design

The suspension that connects m_1 to the substrate via anchors is comprised of four double-folded flexures (Figure 8). Each beam is with length L_{1x} in the folded flexures and it is related to an overall stiffness of :

$$k_{1x} = \frac{4}{2}\left(\frac{1}{2}\frac{3EI}{2\frac{L_{1x}^3}{2}}\right) = \frac{2Etw^3}{L_{1x}^3} \quad (1)$$

where *E* is the Young's Modulus, *I* is the second moment of inertia of the beam crosssection, *t* is the beam thickness, and *w* is the beam width. In this example the following values are used: E=10GPa, t=w=3μm, L_{1x}=100μm, L_{2x}=120μm, L_{2y}=100μm, L_{3y}=120μm.

The mass m_2 is connected to m_1 by four flexures composed of two double folded beams of length L_{2x} and L_{2y} that deform independently in the drive and sense directions. These beams can also be modeled similarly, resulting in m_2 drive and sense direction stiffness values of:

$$k_{2x} = \frac{2Etw^3}{L_{2x}^3} \quad (2)$$

$$k_{2y} = \frac{2Etw^3}{L_{2y}^3} \quad (3)$$

The suspension connecting the mass m_3 to m_2 is made up of four three folded flexures, fixing m_3 with respect to m_2 in the drive direction. With a length of L_{3y} for each beam, the overall stiffness is

$$k_{3y} = \frac{4Etw^3}{3L_{3y}^3} \quad (4)$$

The calculated values for the stiffness are as follows: k_{1x}=1.62N/m, k_{2x}=0.9N/m, k_{2y}=1.62N/m, k_{3y}=0.625N/m.

Design of Damping Estimation

For the driven mass m_1, the total damping in the drive mode can be approximated as the combination of the slide film damping between the mass and the substrate, and the slide film damping between the integrated comb fingers. Assuming an instantaneously developed linear fluidic velocity profile, slide film damping can be modeled as a Couette flow through the formula:

$$c_{1x} = \mu_e \frac{A_1}{z_0} + \mu_e \frac{2N_{comb} l_{comb} t}{y_{comb}} \quad (5)$$

where A_1 is the area of the active mass, z_0 is the elevation of the proof mass from the substrate, t is the thickness of the structure, Ncomb is the number of comb-drive fingers, y_{comb} is the distance between the fingers, and l_{comb} is the overlapping length of the fingers. The effective viscosity is

$$\mu_e = \mu_p p \quad (6)$$

where p is the ambient pressure within the cavity of the packaged device, and μ_p is the viscosity constant for air

$$\mu_p = 3.710^{-4}\left[\frac{kg}{m^2.s.torr}\right] \quad (7)$$

Since there are no actuation and sensing capacitors attached to the mass m_2, the damping coefficients in the drive and sense directions are equal, and they are depended from the Couette flow between the proof mass and the substrate:

$$c_{2x} = c_{2y} = \mu_e \frac{A_2}{z_0} \quad (8)$$

For the mass m3, the total damping in the drive mode results from Couette flow between the mass and the substrate, as well as Couette flow between the air-gap capacitor fingers is:

$$c_{3x} = \mu_e \frac{A_3}{z_0} + \mu_e \frac{2N_{cap} l_{cap} t}{y_{cap}} \quad (9)$$

where A_3 is the area of the passive mass, Ncap is the number of air-gap capacitors, y_{cap} is the distance between the capacitor fingers, and l_{cap} is the overlapping length of the fingers. Damping on m_3 in the sense mode can be estimated as the combination of Couette flow between the proof mass and the substrate, and the Squeeze Film damping between the air-gap capacitor fingers:

$$c_{3y} = \mu_e \frac{A_3}{z_0} + \mu_e \frac{7N_{cap} l_{cap} t^3}{y_{cap}^3} \quad (10)$$

For this example: p=300mtorr, z_0=20μm , Ncomb= 40, y_{comb}=10μm, l_{comb}=25μm, t=3.5μm, N_{cap}=40, l_{cap}=25μm, y_{cap}=10μm and then: μ_e= 0.111, c_{1x}=2850.10^{-6}Ns/m, c_{2x}=c_{2y}=499.10^{-6}Ns/m, c_{3x}=133.2.10^{-6}Ns/m, c_{3y}=88.8.10^{-6} Ns/m.

B. Electrical Design

Electrostatic Actuation

The comb-drives are used as actuation structures, because of the linearity of the generated forces and the ability of applying displacement independent forces. Linearized electrostatic drive forces along the x axis can be achieved by appropriate selection of voltages applied to the opposing comb-drive sets and can be calculated via the formula:

$$F = 4\frac{\varepsilon_0 z_0 N}{y_0} V_{DC} \vartheta_{AC} \quad (11)$$

where V_{DC} is a constant bias voltage, υ_{AC} is an alternate current voltage, z_0 is the finger thickness, y_0 is the finger separation, N is the number of formed capacitors.

If V_{DC}=5V and υ_{AC}=2V, then F=14.16.10^{-9}N.

Electrostatic Sensing

The aim of the sensing is the small capacitance changes resulting from very small displacements of the second mass to be detected and a high sense voltage signal to be provided. For the positive displacement is considered when finger A decreases the capacitance C_{s+} and moves from finger B the capacitance C_{s-} is increased. The finger movement will transfer the displacement to a change in the capacitance, which can be calculated from:

$$C_{s+} = C_{s-} = N\frac{\varepsilon_0 t l}{y_0} \quad (12)$$

where y_0 is the finger separation, l is the fingers' length, t is the finger thickness. The calculated value is:
$C_{s+} = C_{s-} = 1548pF$.

C. Optimization of the Parameters for Performance Enhancement

The dominant force that drives the system in sense direction is the Coriolis force, induced on the passive mass. In order the oscillation amplitude of the passive mass in the sense direction to be maximized, the parameters of the dynamical system have to be optimized. For this purpose: (1) the optimal value of m_2, according to Coriolis force requirement, has to be defined, (2) the resonant frequency w_{22} of the isolated passive mass-spring system has to be determined, (3) the optimal mass ratio $\mu_x=(m_2+m_3)/m_1$ (for the drive mode) and $\mu_y=m_3/m_2$ (for the sense mode) have to be achieved.

From one hand, m_2 has to be large, in order to be achieved a high enough Coriols force, acting on the passive mass, and from the other hand, m_2 has to be small, in order the high oscillation amplitude of passive mass to be achieved. The situation with the resonant frequency w_{22} is the same: the larger Coriolis forces are induced at the higher frequencies, but the oscillation amplitudes are larger at lower frequencies. μ has to be optimized too, because of: μ has to be with a minimal value in order to appropriate insensitivity to damping be achieved, and also μ has to be large to be obtained the wide bandwidth. After this, the optimal values for the frequency ratio $\gamma=w_{22}/w_{11}$ and spring constant k_{1x} of the active mass, has to be obtained.

In the drive mode, the calculated values are the following: w_{1x}=2.54 kHz, w_{2x}= 3KHz, γ_x= 1.1, μ_x= 0.4.

D. Choice of Micromachining Process

In this work, the bulk micromachining process is examined for gyroscope rate MEMS prototyping [9]. The steps in short are the following: (1) The Silicon-on-Insulator (SOI) wafer is a base for the next layers: 100μm thick single-crystalline silicon device layer, 4μm oxide layer, and 400μm e-crystalline silicon handle layer.

(2) Photoresist layer creation, suitable for deep-reactive ion etching (DRIE), after this evaporating the photoresist solvents is applied.

(3) The sample is exposed to UV-light, the mask defines the features of the whole mechanical structure, the exposed photoresist is developed and rinsed with flowing DI water to stop developing. Then, the samples are hard baked in an oven at 900º C.

(4) The DRIE step is performed with Surface Technology Systems in an Inductively Coupled Plasma (ICP) chamber, the etching time was optimized to assure complete through-etching in the smallest trench areas.

(5) The photoresist layer is stripped away after DRIE; the sample is soaked in a 49% HF solution to etch the oxide layer underneath the perforated areas. Etching is stopped with a deionized water dip and then isopropyl alcohol soak, which is immediately, vaporized on a 1000º C hot plate.

V. Conclusion

The rate gyroscope MEMSs are attractive devices for automotive applications realization, because they lead to safe cars: the accidents are decreased, clean cars: the emission of particles is decreased and economical cars: the sensors are reliable, precise, and cost-efficient. In the paper the design concepts of rate gyroscope MEMSs are explored and analyzed. A method for their design is proposed with the main procedure steps and it is used for performing the design of a 4-DOF gyroscope micromachined device. In this way the verification of the proposed design method is done.

Aknowledgment

The research, described in this paper, was carried out within the framework of the Contracts № 091ni034-03/15.05.2009 and № D002-106/15.12.2008.

References

[1] J. Bouchaud. *MEMS Industry and Market Overview*, 2008, http://www.uclouvain.be/cps/ucl/doc/chairemems/documents/MEMS_market_louvain_wtc.pdf
[2] Nanotechnology Group, *Micro-electro-mechanical Systems*, http://knowledgecontext.org/COSMOS/Kubby_MEMS_2007.pdf
[3] P. Ernst, R. Bosch. *MEMS@BOSCH: Automotive applications and beyond*, Automotive Electronics, http://www.mstbw.de/imperia/md/content/mstbw/bestpractice/bosch_mems_12_micromachine_symposium_ernst.pdf
[4] H. Xie, G. Fedder. *Integrated Microelectromechanical Gyroscopes,* Journal Aerospace Engineering, Volume 16, Issue 2, pp. 65-75, April 2003.
[5] D. Sparks, S. Zarabadi, J. Johnson, Q. Jiang. *A CMOS integrated surface micromachined angular rate sensor: It's automotive applications*, 9th International Conference Solid-State Sensors and Actuators, Chicago, IL, June 1997, pp. 851-854.
[6] A. Schofield, A. Trusov, A. Shkel, *Micromachined Gyroscope Design Allowing for Both Robust Wide-Bandwidth and Precision Mode-Matched Operation*, IEEE Sensors Conference, Lecce, Italy, October 2008, pp. 26-29.
[7] W.Geiger, W.U. Butt, A. Gaisser, J. Fretch, M. Braxmaier, T. Link, A. Kohne. *Decoupled Microgyros and the Design Principle DAVED*, IEEE Sensor Journal, 2001, pp.170-173.
[8] Y. Mochida, M. Tamura, K. Ohwada. *A Micromachined Vibrating Rate Gyroscope with Independet Beams for Drive and Detection Modes*, Sensors and Actuators, vol. 80, 2000, pp. 170-178.
[9] S. Lee, S. Park, J. Kim, D. Cho. *Surface/bulk micromachined singlecrystalline-silicon micro-gyroscope*. IEEE/ASME Journal of Microelectromechanical Systems, vol.9, No.4 Dec. 2000, pp. 557-567.